Monthly Notices
of the
ROYAL ASTRONOMICAL SOCIETY

MNRAS **499,** 3071–3084 (2020)
Advance Access publication 2020 September 30

doi:10.1093/mnras/staa3013

Eclipse time variations in the post-common envelope binary V470 Cam

O. Sale,[1] D. Bogensberger,[1,2] F. Clarke[1] and A. E. Lynas-Gray[1,3,4]★

[1]*Department of Physics, University of Oxford, Oxford OX1 3RH, UK*
[2]*Max Planck Institute for Extraterrestrial Physics, D-85748 Garching, Germany*
[3]*Department of Physics and Astronomy, University College London, Gower Street, London WC1E 6BT, UK*
[4]*Department of Physics and Astronomy, University of the Western Cape, Private Bag X17, Bellville 7535, South Africa*

Accepted 2020 September 19. Received 2020 September 19; in original form 2019 December 31

ABSTRACT

Linear or quadratic relations fitted to the time-dependence of post-common envelope binary eclipse times generally give residuals exhibiting a cyclic variation. Among several possible explanations is the presence of one or more orbiting circumbinary objects causing a reflex motion of the binary centre-of-mass, thereby altering the light-travel-time.Twenty new eclipse times for the post-common envelope binary V470 Cam have been obtained; with these and 380 useable eclipse times in the literature, two circumbinary brown dwarfs having orbital periods of 7.87 ± 0.08 and 13.27 ± 0.16 yr were found to give an excellent fit to cyclic residuals resulting from a quadratic ephemeris fit. Irrespective of the excellent fit, it would be premature to claim that the V470 Cam binary is accompanied by two orbiting brown dwarfs; at the very least more eclipse times are needed to confirm the result and other plausible explanations, such as the Applegate mechanism, need eliminating.

Key words: stars: individual: (V470 Cam) – stars: subdwarfs – stars: variables: general.

1 INTRODUCTION

Subdwarf B (sdB) stars are understood to be core-helium burning, retaining in most cases only a thin hydrogen envelope ($\sim 10^{-4}$ $M_\odot$) and constitute blue extensions of horizontal branches seen in Hertzsprung–Russell Diagrams of globular clusters and stars in the field. Heber (2009, 2016) presents contemporary reviews of sdB stars. For more historical reviews we refer the reader to Zwicky (1965a,b), Greenstein (1987), and Lynas-Gray (2004).

Binary population synthesis calculations (Han et al. 2002, 2003; Clausen et al. 2012) show single sdB stars form through the merger of two helium white dwarfs in a binary system; those in binary systems have red giant progenitors whose hydrogen envelope is almost completely removed at or just before the Helium Flash. Wide binaries having a sdB star well-separated from a Main Sequence (MS) companion form from stable or unstable Roche Lobe overflow, and Chen et al. (2013) discuss the observable orbital period distribution that is likely to result. Clausen & Wade (2011) propose an alternative and related channel through which singleton sdB stars may form through the merger of a helium white dwarf and a low-mass hydrogen burning star; the same scenario in a triple system, having a third star initially too far from the merging pair to affect stellar evolution, could also form sdB stars in wide binaries.

In this paper, we were concerned with those sdB stars in close binaries with periods of few hours, the companion typically being a M dwarf; these are understood to form through common envelope evolution (Nelemans & Tout 2005; Davis, Kolb & Willems 2010; Xiong et al. 2017), where companion orbital angular momentum is transferred to a red giant envelope, thereby removing it to leave a sdB star. Companion orbital angular momentum loss is accompanied by orbit shrinkage to leave a close binary. Binaries which are understood to be a consequence of common envelope evolution are generally referred to as post-common envelope binaries (PCEBs) in the literature; the dimensions of the stars and their separation in these systems means that they are easy to identify through their short-period light curves exhibiting eclipses or reflection effects.

Menzies & Marang's (1986) discovery of the first PCEB (HW Vir) allows model-independent first determinations (Wood, Zhang & Robinson 1993; Wood & Saffer 1999; Kiss et al. 2000; Baran et al. 2018) of sdB star physical parameters. Kilkenny, Marang & Menzies (1994) discover the orbital period of the HW Vir binary to be decreasing on the basis of data obtained over a nine-year period. The Kilkenny et al. (1994) discovery and the subsequent discovery of orbital period decreases (and increases) in other PCEB binaries, as Zorotovic & Schreiber (2013) summarise, present an opportunity to examine the nature of PCEBs in more detail. Understanding orbital period changes is crucial to modelling the long-term evolution of PCEB binaries.

The first discovery of a planet outside the Solar System (Mayor & Queloz 1995) attracted immediate attention. In the case of PCEBs, the possibility of orbiting planets presents a possible (although not obvious) explanation for orbital period changes. From a theoretical perspective, Bear & Soker (2014) consider planet formation at the same time as a sdB progenitor, and those planets surviving a subsequent common envelope phase. An alternative scenario which Bear & Soker (2014) also consider is a subsequent formation of planets from residual gas and dust in a PCEB following common envelope evolution.

While Bear & Soker (2014) consider planet formation before common envelope evolution to be more probable from angular momentum considerations, Schleicher & Dreizler (2014) demon-

★ E-mail: tony.lynas-gray@physics.ox.ac.uk

strate the feasibility of planet formation from common envelope ejecta. Furthermore, Schleicher et al. (2015) cannot account for two circumbinary (CB) planetary mass companions assumed as an explanation for eclipse time variations in NN Ser, by a scenario in which both were formed before common envelope evolution. If planets orbit PCEB systems and are responsible for eclipse time variations through light-travel-time changes, further observations of these should in due course help clarify whether they are formed before or after the common envelope stage. Of course, a further possibility is that planets form before and survive the common envelope stage, and further planets subsequently form from the debris.

Before planets outside the Solar System and PCEB period changes had been discovered, Applegate (1992) explains orbital period modulations in binaries as a gravitational coupling of an orbit to shape variations in a magnetically active system star. In the case of PCEB binaries, Völschow et al. (2016) consider the merits of the Applegate and the CB planet hypotheses; they find that the energy required by the former is not available in many PCEB systems and it may only be a minor contributor to orbital period modulations. In a further paper Völschow et al. (2018) consider moderate levels of stellar parameter fluctuations in RS CVn-like systems and find resulting binary period variations the Applegate mechanism predicts to be one to two orders of magnitude lower than observed; they note, however, that the most promising cases where orbital period variation might be explained in this way are those PCEB systems in which the component separation is $\leqslant 1\,\mathrm{R}_{\odot}$.

In a parallel study, Navarrete et al. (2018) investigate the feasibility of the Applegate mechanism, by evolving twelve PCEB binaries with varying secondary masses and rotation rates. A simple dynamo model is applied to secondary radial profiles to investigate a scale at which a predicted activity cycle matches observed modulation periods, quantifying uncertainties involved. Navarrete et al. find the Applegate mechanism to be energetically feasible in five PCEB systems having the highest secondary rotation rate, as a fraction of its critical rotation rate.

As secondaries in PCEB systems are fully convective and magnetic braking is not believed to occur, Chen & Podsiadlowski (2017) explore the consequences of resonant interactions with CB discs; they find that observed orbital period derivatives with respect to time could be explained in this way if CB discs have masses in the range 10^{-4}–$10^{-2}\,\mathrm{M}_{\odot}$. DE CVn is an eclipsing PCEB which Han et al. (2018) find to have an orbital period with a rapid decrease rate, along with a cyclic period oscillation. Han et al. are able to explain the DE CVn period decrease rate if a CB disc is present, following the model Chen & Podsiadlowski propose. To explain the superimposed cyclic period oscillation, Han et al. hypothesise that a giant planet ($\sim 1\,M_{\mathrm{Jup}}$) is orbiting the DE CVn system in a circular orbit of radius $\sim 5.75 \pm 2.02$ au.

Tidal interactions in PCEB systems, and the consequent angular momentum transfer between stellar rotation and their orbits, affecting orbital periods, requires further study. Preece, Tout & Jeffery (2018) find tidal orbit-rotation synchronisation time-scales in PCEB systems to be longer than sdB star lifetimes, even after examining the roles of convective overshooting and dissipation in sdB star cores. From asteroseismic studies the outer 55% of NY Vir is understood to rotate as a solid body and is tidally synchronised with the orbit, but Preece, Tout & Jeffery (2019) fail to explain this with an artificially extended convective core; they suggest a solution may lie in replacing Böhm-Vitense's (1958) Mixing Length Theory of convection with a more sophisticated treatment.

Considerations summarised above led the present authors to appreciate the need for further observations of PCEB system eclipse times. V470 Cam (HS 0705+6700) was selected because from Oxford it is circumpolar [$\alpha(2000) = 07{:}10{:}42.07$ and $\delta(2000) = +66{:}55{:}43.6$] and bright enough ($B \simeq 14.1$) to be observed with a small telescope from a city centre site. Here $\alpha(2000)$ and $\delta(2000)$, respectively, refer to right ascension and declination for the epoch 2000. Twenty new eclipse times are reported, extending an earlier study with the same facilities by Bogensberger, Clarke & Lynas-Gray (2017, 2018). We found that two CB bodies could explain the observed period oscillation.

2 OBSERVATIONS AND REDUCTIONS

V470 Cam was observed with the Philip Wetton Telescope on twelve nights between 2017 November 29 and 2018 February 1. Exactly 3949 images were obtained following the procedure and instrumentation Bogensberger et al. (2017) adopt and who also provide a brief description of the telescope and the site at which it was operated. In our case, images were obtained without a filter (in 'white light') using a 30-s integration time. By accounting for charge coupled device quantum efficiency, atmospheric transmission, and optical surface coatings, we noted that our 'white light' observations were in effect obtained using a 'filter' having an effective wavelength of 6490 Å, a full width at half-maximum of 3400 Å, and a bandpass of 4200–7600 Å.

Data reduction was carried out in the usual way with the CCDPROC package in ASTROPY (Astropy Collaboration et al. 2018). Bias and dark frames were subtracted from science and flat-field frames, a production flat-field frame being assembled from the latter after removal of defects such as cosmic ray hits. Instrumental pixel-to-pixel sensitivity variations in science images were minimised by dividing each of them by the normalised production flat-field frame.

As a comparison star against which V470 Cam magnitudes are differentially corrected for variations in atmospheric extinction and transparency, Bogensberger et al. (2017) choose GSC22 0710387+665708 [$\alpha(2000) = 07{:}10{:}38.72$ and $\delta(2000) = +66{:}57{:}08.2$]. Guide Star Catalog (Lasker et al. 2008) magnitudes indicate that GSC22 0710387+665708 is nearly 2 mag brighter than V470 Cam and separated from it by 86.52 arcsec; it is also isolated in the field, making aperture photometry straightforward. We accordingly adopted the same comparison star. *Gaia* Data Release 2 (DR2) photometry, subsequently published and for which Maíz Apellániz & Weiler (2018) discuss sensitivity curves, gives $G = 14.62$ and $G_{\mathrm{BP}} = 14.45$ for V470 Cam along with $G = 13.36$ and $G_{\mathrm{BP}} = 13.87$ for GSC22 0710387+665708. While confirming our Guide Star Catalog assessment of GSC22 0710387+665708 as a suitable comparison star, *Gaia* magnitudes highlight a long-standing problem with sdB star differential photometry, which is that an observer almost always depends on making comparisons with a redder star.

Instrumental magnitudes for V470 Cam and the selected comparison star (GSC22 0710387+665708) were extracted from processed frames with the PHOTOUTILS package in ASTROPY. A circular aperture having a 7 arcsec radius was centred on the star of interest, the corresponding background correction being obtained using a concentric annulus having inner and outer radii of 21 and 28 arcsec, respectively. Our chosen circular aperture, while smaller than would normally be used, was chosen to eliminate any contribution from GSC22 0710400+665538, a $V \sim 17.5$ red star separated from V470 Cam by 14 arcsec. A differential correction for each V470 Cam magnitude was provided by the comparison star magnitude; this eliminates dependencies on airmass, sky transparency, and seeing variations.

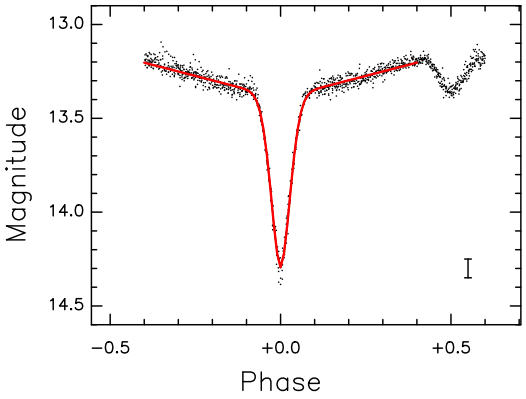

Figure 1. Phased 'white light' curve for V470 Cam based on all our observations and the Drechsel et al. (2001) ephemeris expressed in terms of Barycentric Dynamical Time (see Equation 2). The characteristic error in each magnitude is displayed in the lower right-hand corner. The superimposed red curve is a modified Gaussian fit, following Bogensberger et al. (2017), referred to in the text as the 'master light curve'.

As our observations were to be interpreted along with literature eclipse times various authors obtain over nearly two decades, with five leap seconds (McCarthy, Hackman & Nelson 2008) being introduced during this period (2006 January 1, 2009 January 1, 2012 July 1, 2015 July 1, and 2017 January 1), we expressed our times of observation (and those of other authors where a correction was necessary) as Barycentric Dynamical Time (BJD_{TDB}; Eastman, Siverd & Gaudi 2010). The BJD_{TDB} at which primary eclipse number N occurs is given by the Pulley et al. (2018) ephemeris:

$$\begin{aligned} BJD_{TDB} &= 245\,1822.76155(5) + 0.095646609(4)N \\ &\quad +5.5(9) \times 10^{-13}\,N^2 + \tau_3, \end{aligned} \tag{1}$$

where digits in parentheses give (here and elsewhere in this paper) standard deviations (e.g. $245\,1822.76155 \pm 0.00005$), τ_3 being a cyclical light-travel-time to be discussed further below. Although Equation (1) includes a non-zero quadratic term, suggesting a very small increase in the binary orbital period since 2001, the adapted Drechsel et al. (2001) ephemeris,

$$BJD_{TDB} = 245\,1822.76055(22) + 0.09564665(39)N, \tag{2}$$

has coefficient errors which are small enough to allow an unambiguous assignment of N to primary eclipses we observed in 2017 and 2018. The binary orbital period was therefore adopted as a constant over the two-month period during which our data were obtained and we phased our observations using Equation (2) to obtain the master light curve presented in Fig. 1, interpreting N in Equation (2) outside mid-primary eclipse as a phase.

Following Bogensberger et al. (2017), the light curve defined by all our phased observations was fitted by a modified Gaussian of the form

$$m = a \exp\left(-\left|\frac{\phi}{w}\right|^p\right) + M_0 + r\,|\phi|\,, \tag{3}$$

where m is the magnitude observed at phase ϕ. In the case of the Fig. 1 master-light-curve, values obtained for fit parameters are listed in Table 1, where a is the primary eclipse depth, M_0 the magnitude at $\phi = 0$ if there were no eclipse, w the primary eclipse half-width, and r the reflection effect gradient. Phased observations were plotted in Fig. 1 with the modified Gaussian fit shown as the superimposed red curve; both have been corrected for a small phase zero-point offset arising from phasing based on Equation (2).

Table 1. Master-light-curve primary eclipse fit parameters.

Parameter	Value (error)	Units
a	+0.902(9)	mag
w	+0.03950(33)	cycles
p	+1.855(40)	
M_0	13.392(4)	mag
r	− 0.4713(4)	mag cycle^{-1}

Individual mid-primary eclipse times are defined by the primary eclipse profile and the adjacent light-curve shape, as it was unlikely that any mid-exposure time was also coincident with a time of primary eclipse. Following the Bogensberger et al. (2017) procedure, a modified Gaussian was fitted to each individual primary eclipse and the result cross-correlated against the master-light-curve to establish the corresponding phase shift. Observed (O) BJD_{TDB} times of primary eclipse were then recovered using Equation (2).

As Pulley et al. (2018) identify a non-zero quadratic term in their ephemeris, we used weighted linear least squares to fit the 400 available eclipse times (380 taken from the literature and the additional 20 reported in this paper) to obtain

$$\begin{aligned} BJD_{TDB} &= 245\,1822.75909(2) + 0.0956466807(8)N \\ &\quad +2.448(89) \times 10^{-13}\,N^2. \end{aligned} \tag{4}$$

Our purpose in deriving Equation (4) was to minimise random errors in calculated (C) BJD_{TDB} eclipse times and (O − C) BJD_{TDB} residuals derived from them. No cyclical terms were included in Equation (4) as the intention was only to account for the binary orbital period and its small change over the last two decades. Cyclical corrections were to be investigated as light-travel-time changes, caused by the reflex motion of the binary centre-of-mass as a consequence of orbiting bodies as discussed below.

3 ANALYSIS OF RESULTS

Departures from a linear or quadratic ephemeris for V470 Cam are noted by several authors (Qian et al. 2009, 2010, 2013; Beuermann et al. 2012; Bogensberger et al. 2017, 2018; Pulley et al. 2018; Faillace et al. 2019). Generally, the approach has been to model (O − C) residuals (ΔT) using an equation of the form

$$\Delta T = c_0 + c_1\,N + c_2\,N^2 + \tau(N), \tag{5}$$

where $\tau(N)$ is a cyclic term representing light-travel-time changes caused by the reflex motion of the binary centre-of-mass due to an orbiting third body. Neglecting $\tau(N)$ in determining ephemeris coefficients means that they have systematic errors represented by c_0, c_1, and c_2. In this paper, we have used the eclipse number (N) as the independent variable; it is related to time expressed as BJD_{TDB} through Equation (2).

For the case of a third body in a circular orbit,

$$\tau(N) = A \sin\left[(2\pi\,N/\Pi) - \phi\right], \tag{6}$$

and for an elliptical orbit it is customary to follow Irwin (1952, his equation 3) that leads to

$$\tau(N) = A\left[(1-e^2)^{1/2} \sin E \cos\omega + \cos E \sin\omega\right], \tag{7}$$

with the eccentric anomaly (E) given by the solution to Kepler's Equation,

$$\frac{2\pi}{\Pi} N - \phi = E - e \sin E. \tag{8}$$

Table 2. Ephemeris and reflex motion orbital parameters.

Parameter symbol	Circular orbits parameter value (SD)	Elliptical orbits parameter value (SD)	Units
a_0	$1.82276124(11) \times 10^{+03}$	$1.822761527(43) \times 10^{+03}$	d
a_1	$9.56466400(78) \times 10^{-02}$	$9.56466303(11) \times 10^{-02}$	d cycle^{-1}
a_2	$2.3(1.1) \times 10^{-13}$	$3.82(98) \times 10^{-13}$	d cycle^{-2}
Π_1	$2.936(25) \times 10^{+04}$	$3.002(29) \times 10^{+04}$	cycles
ϕ_1	$1.300(77) \times 10^{+00}$	$-2.10(36) \times 10^{+00}$	rad
A_1	$-7.78(17) \times 10^{-04}$	$8.54(18) \times 10^{-04}$	d
e_1		$7.9(3.7) \times 10^{-02}$	
ω_1		$1.9(3.7) \times 10^{-01}$	rad
Π_2	$4.83(13) \times 10^{+04}$	$5.063(61) \times 10^{+04}$	cycles
ϕ_2	$-9.(14.) \times 10^{-02}$	$-1.64(11) \times 10^{+00}$	rad
A_2	$8.24(32) \times 10^{-04}$	$-7.54(18) \times 10^{-04}$	d
e_2		$4.65(42) \times 10^{-01}$	
ω_2		$-1.44(11) \times 10^{+00}$	rad
$\sqrt{2\chi^2}$	56.24	50.08	
$\sqrt{2n-1}$	27.95	27.80	
n	391	387	
BIC – $2K$	1635.596	1331.730	

Here A is an amplitude in days, ϕ a phase in radians, Π an orbital period in cycles, e an orbital eccentricity, and ω a longitude of periastron passage in radians.

As Pulley et al. (2018, their fig. 3) and Faillace et al. (2019, their fig. 1) point out, measurements obtained since 2017 show that equations like Equation (5) can no longer be used to model ΔT. Use of systematic corrections c_0, c_1, and c_2 was also considered unsatisfactory. We therefore attempted to model $\mathrm{BJD_{TDB}}$ by supposing the V470 Cam binary to be accompanied by two orbiting bodies and simultaneously determining ephemeris coefficients; in this case Equation (5) became

$$\Delta T = a_0 + a_1\, N + a_2\, N^2 + \tau_1(N) + \tau_2(N), \tag{9}$$

where $\tau_1(N)$ and $\tau_2(N)$ represent contributions each orbiting body makes to the light-travel-time caused by the reflex motion of the V470 Cam binary centre-of-mass. Unknown parameters in Equation (9) were determined using the adaptive Markov Chain Monte Carlo (MCMC) sampling routine by Laine & Tamminen (2008). Samples were obtained assuming both circular and elliptical orbits using Equations (6)–(9). In the latter case, solutions to Kepler's Equation were computed with Odell & Gooding's (1986) routine EKEPL2. We made the simplifying assumption that all observations are independent and have equal weight; this was subsequently justified by the satisfactory representation of observations that we obtained.

To obtain orbital parameter priors we used the 'ordinary least squares' option in the routine ODRPACK95 (Zwolak, Boggs & Watson 2007) to fit (O − C) residuals obtained by subtracting Equation (4) predictions from observed $\mathrm{BJD_{TDB}}$ values, using Equation (5) with $\tau(N)$ replaced by $\tau_1(N) + \tau_2(N)$. Again, solutions were obtained for assumed circular and elliptical orbits. Priors for ephemeris coefficients were those in Equation (4).

For both the circular and elliptical orbit cases, we carried out MCMC sampling in ten steps. The starting point for the first step was assumed priors, a unit covariance matrix, and a squared mean variance of 10^{-10} (i.e. each $\mathrm{BJD_{TDB}}$ eclipse time had been determined to a precision of $\simeq 10^{-5}$ d). All subsequent steps started from the result of the one before.

In calculating each step, we generated a chain of 5×10^6 samples. The first 10^6 samples were 'burn in'; these were followed by 10^6 adaptation steps and then a further 3×10^6 sampling steps. Convergence was understood to have been achieved well before the tenth step and this was tested by means of the autocorrelation time as Foreman-Mackey et al. (2013) recommend. Goodman & Weare's (2010) program ACOR gave autocorrelation times of 1.49717 and 1.7291 steps for the circular and elliptical orbit cases, respectively; as these were very much less than the chain length, we considered convergence to have been achieved. For the elliptical orbit case only, we then generated a short chain of 10 000 samples, without 'burn in' or adaptation and plot parameter correlations and distributions obtained as corner plots in Figs B1–B3.

Means and standard deviations from the 5×10^6 samples in the last step chain gave estimates for ephemeris and orbital parameters which we have listed in Table 2. Table 2 ephemeris coefficients gave calculated eclipse times from which we obtained (O − C) residuals plotted in Fig. 2 as single points, and listed in Table A1. Associated error bars were obtained from standard deviations in observed $\mathrm{BJD_{TDB}}$ eclipse times, and those in our MCMC ephemeris coefficients. The left-hand peak in Fig. 2 is higher than the corresponding peak in Bogensberger et al. (2017, their fig. 2) because $\mathrm{BJD_{TDB}}$ has now been used to express times at which Németh, Kiss & Sarneczky (2005) observe eclipses.

In Table 2, the left-hand column identifies parameters by symbols used in Equations (6)–(9); subscripts '1' and '2' appended to parameters Π, ϕ, A, e, and ω associate them with the first and second orbiting bodies (OB1 and OB2), respectively. The right-hand column gives the units in which parameter values and their standard deviations are expressed. For example an OB1 orbital period was found to be $(3.002 \pm 0.029) \times 10^4 \times 0.09564665 = (2871 \pm 28)$ d, where for consistency the conversion has been carried out using the Equation (2) binary orbital period.

Evaluating $\tau_1(N) + \tau_2(N)$ (see Equation 9) with Table 2 orbital parameters gave a predicted (O − C), at each eclipse number N, for both circular and elliptical orbits; these were plotted as thin lines in Fig. 2. Differences δ(O − C) between observed and predicted (O − C) values were plotted as single points in lower panels. We have added $\sqrt{2\chi^2}$, $\sqrt{2n-1}$, and n to Table 2; $\sqrt{2\chi^2}$ has a Gaussian distribution with mean $\sqrt{2n-1}$ and unit variance, where n is the number of degrees of freedom.

As may be seen in Fig. 2, having ensured that all eclipse times used to determine (O − C) residuals were expressed as $\mathrm{BJD_{TDB}}$ times, the assumption of two orbiting bodies gave what appeared

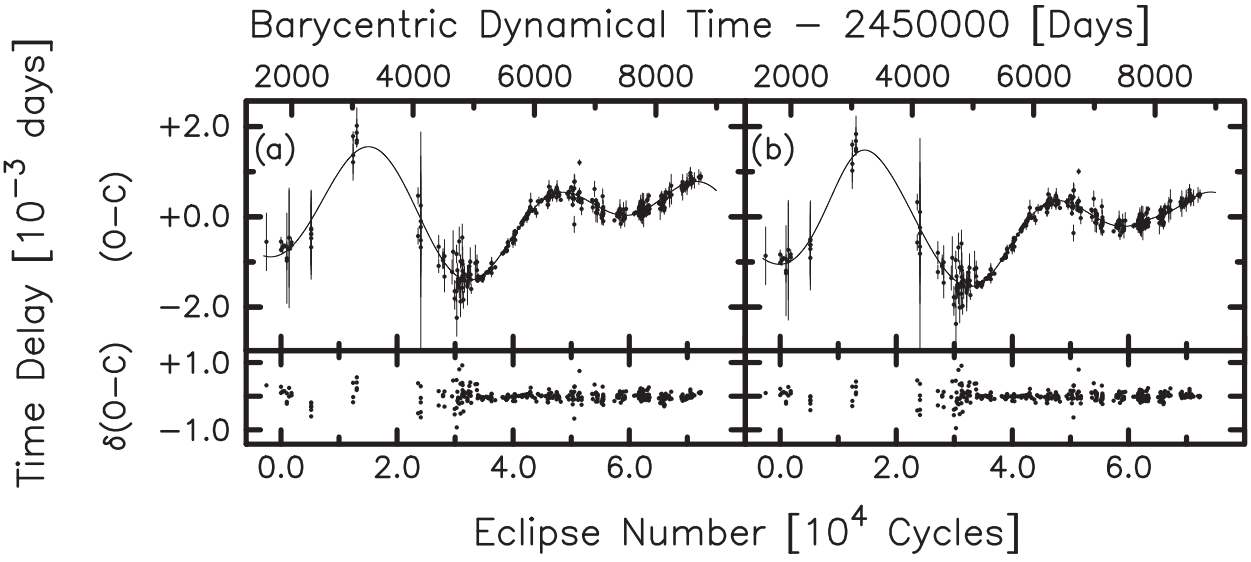

Figure 2. Ephemeris calculations (C) subtracted from observed (O) eclipse times and plotted against eclipse number in the upper panels. Corresponding BJD_{TDB} times were plotted along the upper abscissa axis, the first plotted observation (Beuermann et al. 2012) being obtained in 2000 February and the last (Faillace et al. 2019) in 2019 September. As ephemeris coefficients were determined with orbital parameters, (O − C) values were dependent on the assumption of (a) circular (left-hand panels) and (b) elliptical (right-hand panels) CB orbits. Values for (O − C) were predicted (thin line) assuming two CB bodies orbiting in (a) circular and (b) elliptical orbits; residuals (δ(O − C)) in the sense (O − C) minus its prediction were plotted in smaller lower panels. Standard deviations in (O − C) are shown as error bars in the upper panels, along with fits for assumed CB orbit geometries.

to be an excellent fit to these data. But it can be seen in the Fig. 2 lower panels that the δ(O − C) residuals are typically a factor of 3–4 larger than standard deviation error bars, indicating that there is information in the data that our analysis has not extracted. Confirmation was provided by the statistic $\sqrt{2\chi^2} \gg \sqrt{2n-1}$. The assumption of elliptical orbits gave a superior fit to the data at the $56.24 - 50.08 = 6.16\sigma$ level.

Schwarz (1978) introduces the Bayesian Information Criterion (BIC), which Liddle (2007) discusses in the context of astronomical applications. We have made a further assessment of whether the data indicate elliptical rather than circular orbits using BIC, details and the definition of K being provided in Appendix C. BIC determinations for both cases have been included in Table 2, values $\gg$0.0 again reflect a χ^2 larger than expected for models which extract all available information from the data. The difference BIC(elliptical) − BIC(circular) = −303.866 favours the adopted assumption of elliptical orbits.

Inherent in the use of Equation (9) was the assumption that OB1 and OB2 contributions to the light-travel-time may be treated independently and that there is no detectable interaction between them. Moreover, OB1 and OB2 were considered to orbit the centre-of-mass of the eclipsing binary as though it were a point mass. While there are two points ($N = 50\,525.5$ and $N = 51\,414$) plotted in Fig. 2 that are obviously inconsistent (as established by their error bars) with either fit, there are three other eclipses ($N = 1409$, $N = 30\,149$, and $N = 30\,150$) completely excluded from our analysis as they are identified as giving large residuals in earlier papers (Qian et al. 2009; Bogensberger et al. 2017). Large residuals are currently unexplained and the possibility of a transient interaction between OB1 and OB2 cannot be ruled out, and neither can a breakdown of the eclipsing binary point mass assumption when OB1 or OB2 is at or near periastron. Justification for the assumptions made, in so far as these reflect reality, came from the resulting high-quality fits shown in Fig. 2.

Given that OB1 and OB2 orbit the centre-of-mass of the eclipsing binary as though it were a point mass, and without interaction between them, we followed Qian et al. (2013) and used

$$f(m) = \frac{4\pi^2\,(a\sin i)^3}{G\,\Pi^2} = \frac{(m\sin i)^3}{(M_s + M_c + m)^2} \tag{10}$$

to calculate mass functions $f(m)$ for OB1 and OB2 from which their corresponding minimum masses were obtained. $M_s = 0.48\ M_\odot$ and $M_c = 0.13\ M_\odot$ were, respectively, masses for the hot subdwarf and its companion, numerical values being those Drechsel et al. (2001) obtain from their analyses of the eclipsing binary light and radial velocity curves. In Equation (10), i is the inclination of the orbital plane of a CB orbiting body of mass m and which on its own would induce the eclipsing binary centre-of-mass to move in an elliptical orbit of semimajor axis a about the system barycentre. Induced light-travel-times would be eclipsing binary centre-of-mass displacement vectors projected on to an observer's line-of-sight and divided by the speed of light (c). For OB1 and OB2 (distinguishing between them with subscripts '1' and '2'), we obtained, following Hilditch (2001, his equation 2.57),

$$\tau_{1,2}(N) = \frac{a_{1,2}\sin i_{1,2}}{c}\,\frac{(1-{e_{1,2}}^2)\sin\left[\theta_{1,2}(N)+\omega_{1,2}\right]}{\left[1+e_{1,2}\cos\theta_{1,2}(N)\right]}, \tag{11}$$

where $\theta_{1,2}(N)$ are the corresponding true anomalies related to eccentric anomalies by

$$\cos\theta_{1,2}(N) = \frac{\cos E_{1,2}(N) - e_{1,2}}{(1 - e_{1,2}\cos E_{1,2}(N))}, \tag{12}$$

which in turn are given through mean anomalies,

$$M_{1,2}(N) = \frac{2\pi}{\Pi_{1,2}}N - \phi_{1,2}, \tag{13}$$

and Kepler's Equation (8). Using Equations (8) and (11)–(13), we located maximum absolute values of

$$\tau_1 = (1.012 \pm 0.029)\,a_1\sin i_1/c \tag{14}$$

Table 3. System parameters and maximum contribution to light-travel-time (LTT) across the V470 Cam binary centre-of-mass reflex orbit.

System parameter	Orbiting body 1 (OB1)	Orbiting body 2 (OB2)
Orbital Period (Π – yr)	7.87(8)	13.27(16)
LTT (s)	72(7)	45.0(1.9)
Mass Function ($f(m)$ – $M_\odot$)	$5.0(5) \times 10^{-5}$	$4.1(0.5) \times 10^{-6}$
Minimum Mass ($m \sin i$ – $M_\odot$)	0.027(3)	0.0118(5)
Minimum Semimajor axis (au)	3.27(2)	4.71(4)
Longitude of the Ascending Node (rad)	1.7(5)	4.53(15)

and

$$\tau_2 = (1.459 \pm 0.043)\, a_2 \sin i_2 / c \qquad (15)$$

at $N \simeq 11\,500$ which corresponded with the observed maximum (O − C) in Fig. 2. With E_1 and E_2 obtained from solutions of Kepler's Equation for $N = 11\,500$, Table 2 orbital parameters substituted in Equation (7), resulted in respective maximum reflex motion light-travel-times OB1 and OB2 induce in the V470 Cam binary of $\tau_1 = 72(7)$ s and $\tau_2 = 45.0(1.9)$ s. Having determined τ_1 and τ_2, Equations (14) and (15) gave $a_{1,2} \sin i_{1,2}$. Minimum masses $m_{1,2} \sin i_{1,2}$ for OB1 and OB2 were then calculated from Equation (10) from which their minimum orbital semimajor axes followed, assuming $M_s + M_c = 0.61\,M_\odot$ as discussed above.

An orbiting body recedes with maximum velocity from an observer when located at its orbital ascending node; as Hilditch (2001, his equation 2.45) explains, this occurs when $(\theta(N) + \omega) = 0$. We calculated $(\theta(N) + \omega)$ for $N = 1, 2, \ldots, 80\,000$ and found $(\theta(N) + \omega) = 0$ for OB1 and OB2 at $N = 12\,322$ and $N = 9524$, respectively. Longitudes of ascending nodes for OB1 and OB2 were then given by

$$\Omega_{1,2} = \frac{2\pi N}{\Pi_{1,2}} + \omega_{1,2}, \qquad (16)$$

where an additional adjustment of $\pm\pi$ was needed because determinations had been made for reflex motion orbits. We have summarised our results in Table 3.

4 DISCUSSION

Qian et al. (2009) publish a third body orbital period of 7.15 yr, modelling the V470 Cam light-travel-time change by assuming a single CB object to be responsible. Making the same assumption, as additional eclipse time measurements become available, subsequent third body orbital period determinations are 15.7 yr (Qian et al. 2010), 8.06 yr (Çamurdan, Zengin Çamurdan & İbanoğlu 2012), 8.41 yr (Beuermann et al. 2012), 8.87 yr (Qian et al. 2013), and 11.77 yr (Bogensberger et al. 2017). Discounting the Qian et al. (2010) period which Pulley et al. (2018) propose to be a typographical error (7.15 yr being intended), there is a steady increase in derived period as more eclipse time measurements become available. Additional data which Pulley et al. (2018) secure rule out a one-body solution and prompted our two-body solution; with the hindsight this provided, it became clear that the influence of OB2 ($\Pi_2 = 13.3$ yr) would be more and more important as more eclipse time measurements are added and hence the drift towards longer one-body periods in the above-cited papers.

Near-infrared fluxes for V470 Cam were obtained at effective wavelengths of 1.25, 1.65, and 2.16 μm using the Cohen, Wheaton & Megeath (2003) calibration of the Two Micron All Sky Survey (2MASS; Skrutskie et al. 2006); these gave consistent estimates for the angular radius (α) of the V470 Cam hot subdwarf with a mean $\alpha = 3.90(3) \times 10^{-12}$ rad, when ratioed with the corresponding ($T_{\rm eff} = 29\,000$, $\log g = 5.4$ and $N({\rm He})/N({\rm H}) = 2.0 \times 10^{-3}$) model stellar atmosphere fluxes taken from the Han, Podsiadlowski & Lynas-Gray (2007) grid. The interstellar extinction model of Amôres & Lépine (2005) indicates a total V-band extinction of $A_V = 0.15 \pm 0.15$ in the direction of V470 Cam, which in the J-band (Fitzpatrick 1999) corresponds to $A_J = 0.04 \pm 0.04$; therefore, neglecting interstellar extinction introduces a probable systematic error in the angular radius of ∼4%.

Bailer-Jones et al. (2018) list a distance of 1.195(73) kpc for V470 Cam which, with the above angular radius, gave a radius $R_s = 0.206(13)\,R_\odot$ for the hot subdwarf primary. Using $\log g = 5.4 \pm 0.1$ as Drechsel et al. (2001) determine, we then deduced a hot subdwarf mass of $M_s = 0.39(0.10)\,M_\odot$; this was smaller than the $M_s = 0.483\,M_\odot$ Drechsel et al. obtain, although consistent within error limits. Our R_s was also smaller than the Drechsel et al. value of $R_s = 0.230\,R_\odot$.

Drechsel et al. (2001) derive a mass function $f(m) = 0.00626 \pm 0.00081\,M_\odot$ for the V470 Cam eclipsing binary. The M_s derived above then implies a companion mass $M_c = 0.12(2)\,M_\odot$. Equation (10) would then imply OB1 and OB2 minimum masses of 0.0243(33) and 0.0103(14) $M_\odot$, respectively; the higher errors, compared with those in Table 3, follow because error estimates in *Gaia* distance-based masses were propagated through the calculation. The conclusion that OB1 and OB2 were brown dwarfs, if present, was not affected.

Adopting $M_s = 0.39(0.10)\,M_\odot$, and circular orbits for both stars about the binary centre-of-mass, the orbital radii deduced were $a_s = 0.162(7)\,R_\odot$ and $a_c = 0.54(7)\,R_\odot$ for the primary and secondary, respectively. The corresponding separation of centres-of-mass was then $a = 0.70(7)\,R_\odot$. Noting that $a_s < R_s$, between primary and secondary eclipse, the radiating hemisphere of the primary was found to move $0.087(30)\,R_\odot$ towards an observer. The change in light-travel–time between primary and secondary eclipse was therefore 0.20(7) s.

We have followed other observers and used their times of secondary eclipse, reproduced in Table A1, in our analysis without regard for the difference in light-travel-time between primary and secondary eclipse. As eclipse times are determined to a precision of ∼1 s, our approach was justified in that a systematic light-travel-time shift of 0.2 s was not detectable; this was confirmed by close inspection of data plotted in Fig. 2. Our study was compared with *Kepler* satellite observations of HW Vir (another PCEB) by Baran et al. (2018) who in this case observe a light-travel-time difference between primary and secondary eclipse of 1.62 s and use this to infer an improbably low mass of $0.26\,M_\odot$ for the HW Vir primary.

For our two-orbiting-body explanation of V470 Cam eclipse time variations to be plausible, it must be established that OB1 and OB2 have dynamically stable orbits about the central binary for a time comparable with the hot subdwarf primary evolution timescale (∼10^8 yr). Horner et al. (2012) investigate the orbital stability of two planets Lee et al. (2009) report to be orbiting the PCEB binary HW Vir. Horner et al. improve the light-travel-time analysis by Lee et al. and use Chambers's (1999) hybrid symplectic integrator program MERCURY6 to show that even in this case the required orbits for HW Vir planets are dynamically unstable, one or the other being ejected from the system after a few hundred years.

NY Vir is another well-studied PCEB binary for which Lee et al. (2014) report two CB planets. With eighteen new primary minima

time observations, Song et al. (2019) obtain orbits for the Lee et al. planets which are stable for at least 10^8 yr although they note that if either eccentricity is increased from 0.15 to 0.2 (within error limits for the inner planet), then the solution becomes unstable in 10^6 yr. As with V470 Cam, available eclipse times do not encompass a time interval long enough to be confident that eclipse time variations are due to light-travel-time changes, arising from a reflex motion of the binary centre-of-mass.

In the case of V470 Cam, we followed Horner et al. (2012) and Song et al. (2019) by assuming the central eclipsing binary could be regarded as a single object of (in our case) 0.61 $M_\odot$ at its centre of mass. Orbital elements given in Tables 2 and 3 were then adopted. For OB1 we selected an orbital inclination of 90.°0; that is, the orbital plane lies in an observer's line-of-sight. Kepler's Third Law then sets the OB2 orbital inclination to be 79.°7(9), given the semimajor axes and periods determined. Using MERCURY6 (Chambers 1999) with an ejection distance of 1000 au showed that OB2 would be ejected after ∼500 yr. Adopting the smaller hot subdwarf mass of 0.39 $M_\odot$ determined above, along with consequential changes, would result in OB2 being ejected after ∼1800 yr.

Dynamical instability of two-body CB systems in the cases of HW Vir and V470 Cam, and questionable stability in the case of NY Vir, requires serious consideration of alternative explanations for observed PCEB orbital period modulation. Lanza (2020) presents a new model based on an angular momentum exchange between the spin of an active component and orbital motion. Spin–orbit coupling, as Lanza proposes, is not due to tides, where the time-scale is too long, but the result of a non-axisymmetric component of the gravitational quadrupole moment which arises in an active star due to its persistent non-axisymmetric magnetic field. M dwarf secondaries in PCEB systems are obvious active star candidates, although the Lanza model gives observable orbital period modulation only in systems that are close to tidal synchronisation.

Geier et al. (2010) discuss the synchronisation between rotation and orbital motion in close binary systems having a hot subdwarf primary; they obtain projected rotational velocities spectroscopically or from the literature. Among the forty systems Geier et al. study, thirty are found to have a hot subdwarf rotating synchronously with orbital motion. Specifically, hot subdwarfs in the V470 Cam, HW Vir, and NY Vir systems are found to be rotating synchronously with the orbital motion and their companions identified as Main-Sequence M dwarfs. As a consequence the Lanza model needs to be considered as a plausible explanation of observed orbital period modulation in these cases.

Observed PCEB orbital period rates of change ($\dot{\Pi}$) are $\dot{\Pi}_{\rm HW\,Vir} = -9.6(8) \times 10^{-9}\,{\rm d\,yr^{-1}}$ (Horner et al. 2012) and $\dot{\Pi}_{\rm NY\,Vir} = +2.05(18) \times 10^{-8}\,{\rm d\,yr^{-1}}$ (Song et al. 2019) suggest that at least one PCEB component in these systems is not rotating synchronously with orbital motion. A similar result was obtained for V470 Cam, the quadratic term in Equation (4) gave $\dot{\Pi}_{\rm V470\,Cam} = 2.9(7) \times 10^{-9}\,{\rm d\,yr^{-1}}$. Non-zero values of $\dot{\Pi}$ can be understood in terms of orbital evolution and the transfer of angular momentum between an orbit and rotation of one or both binary components. Any angular momentum transfer as suggested would be indicative of tidal locking not having yet been completely established as Geier et al. (2010) propose. If correct then we have the circumstances in which the Lanza (2020) orbital period modulation model could operate. Orbital period modulation through the Lanza model would imply future $\dot{\Pi}$ changes in sign; it would therefore be important to secure future eclipse time measurements for HW Vir, NY Vir, and V470 Cam in particular to see if higher order ephemeris terms can be identified.

5 CONCLUDING REMARKS

We have collected all useable eclipse time measurements for V470 Cam available in the literature at the time of writing and obtained twenty new measurements ourselves; fitting their time-dependence to determine a quadratic ephemeris gave residuals which exhibited a clear cyclic pattern. Two orbiting CB brown dwarfs were found to provide a reflex motion of the V470 Cam binary centre-of-mass, which resulted in light-travel-time changes providing an excellent agreement with those implied by the quadratic ephemeris residuals. In principle we have therefore demonstrated that the V470 Cam binary is accompanied by two orbiting brown dwarfs.

To reach such a conclusion at this early stage would be premature for three reasons.

(i) Eclipse time measurements have been obtained over a period of less than twenty years that is barely longer than the orbital period of the outer brown dwarf (13.3 yr). There can be no certainty that future eclipse time measurements will be consistent with our two brown dwarf model. At the very least, more eclipse time measurements over the coming decades would be needed.

(ii) The two brown dwarf model proposed was found to be dynamically unstable on a time-scale of $\sim 10^3$ yr. While the plausibility of our model is greatly diminished, it is not necessarily eliminated. Brown dwarf magnetic fields are well studied, as for example Kao et al. (2018) discuss; if OB1 and OB2 are brown dwarfs, they would be expected to interact magnetically with the M dwarf and sdB binary. M dwarfs are understood to be fully convective and have magnetic fields as for example Reiners (2012) summarises. The sdB component of the V470 Cam binary could also have a magnetic field as O'Toole et al. (2005) find in those hot subdwarfs for which they present polarisation measurements. Magnetic interactions between OB1, OB2, and the central PCEB have not been taken into account and whether these could contribute to the stability of OB1 and OB2 orbits remains to be investigated.

(iii) Other possible explanations for cyclic eclipse time departures from our quadratic ephemeris have not been fully investigated, and certainly not eliminated. Conventional wisdom suggests PCEB orbits have had time to circularise and a sdB primary rotation is tidally locked to its orbital period; if so, apsidal motion does not occur. However, Preece et al. (2018) find synchronisation time-scales for PCEB systems with a sdB primary to exceed sdB lifetimes stellar evolution calculations suggest. Orbits may therefore be elliptical with very small eccentricities, and apparent cyclic period changes due to apsidal motion need to be considered. As an example, Baran et al. (2018) need to adopt $e \cos\omega \simeq 0.0001$ for the PCEB HW Vir if they are to reconcile their observed Rømer delay of 1.62 s with the sdB canonical mass of $\simeq$0.47 $M_\odot$. In the case of V470 Cam our quadratic ephemeris indicates that its components may not be tidally locked and their orbits about the binary centre of mass may not have circularised. Among the primary eclipses listed in Table A1, twenty are accompanied by times for the subsequent secondary eclipse; we found the mean time difference between these to be 0.5005 ± 0.0015 cycles. There was therefore no indication from our analysis of non-circularisation of V470 Cam binary orbits, but a small eccentricity would not be detectable as Baran et al. explain. A future study should nonetheless attempt to account for our observed period changes, along with any inferred from new data, as being a consequence of apsidal motion in the PCEB orbits as an alternative to reflex motion caused by CB objects.

Evryscope (Law et al. 2015, 2016) images the entire sky, weather permitting, with a 2-min cadence and should provide future eclipse

time measurements for V470 Cam and other PCEB systems which are bright enough. Understanding PCEB binaries, and whether or not they are in some cases accompanied by orbiting planets or brown dwarfs, is important for a more general understanding of the late stages of stellar evolution. Ratzloff et al. (2020) give an overview of results from Evryscope observations of PCEB systems in the Southern Sky, obtained between 2016 January and 2018 June; these observations are continuing and a Northern Sky extension is anticipated.

ACKNOWLEDGEMENTS

Observations reported in this paper were obtained with the Philip Wetton Telescope, provided by Mr Philip Wetton through a very generous benefaction and operated by the University of Oxford. Computing facilities owned by the University of Oxford and University College London were also used. The authors are indebted to Dr D. Pulley for invaluable discussion and for the provision of eclipse times in advance of publication and to an anonymous referee whose comments guided us to make substantial improvements to this paper.

DATA AVAILABILITY

In order to assist future studies, we have provided Table A1 as a machine-readable ASCII file in supplementary material presented with the online version of this paper. From left to right the columns are eclipse number, barycentric dynamical time, barycentric dynamical time standard deviation, and (O − C) residuals we determined. Times have been expressed in days.

REFERENCES

Amôres E. B., Lépine J. R. D., 2005, AJ, 130, 659
Applegate J. H., 1992, ApJ, 385, 621
Astropy Collaboration et al., 2018, AJ, 156, 123
Bailer-Jones C. A. L., Rybizki J., Fouesneau M., Mantelet G., Andrae R., 2018, AJ, 156, 58
Baran A. S. et al., 2018, MNRAS, 481, 2721
Bear E., Soker N., 2014, MNRAS, 444, 1698
Beuermann K. et al., 2012, A&A, 540, A8
Bogensberger D., Clarke F., Lynas-Gray A. E., 2017, Open Astron., 26, 134
Bogensberger D., Clarke F., Lynas-Gray A. E., 2018, Open Astron., 27, 75
Böhm-Vitense E., 1958, Z. Astrophys., 46, 108
Çamurdan C. M., Zengin Çamurdan D., İbanoğlu C., 2012, New Astron., 17, 325
Chambers J. E., 1999, MNRAS, 304, 793
Chen W.-C., Podsiadlowski P., 2017, ApJ, 837, L19
Chen X., Han Z., Deca J., Podsiadlowski P., 2013, MNRAS, 434, 186
Clausen D., Wade R. A., 2011, ApJ, 733, L42
Clausen D., Wade R. A., Kopparapu R. K., O'Shaughnessy R., 2012, ApJ, 746, 186
Cohen M., Wheaton W. A., Megeath S. T., 2003, AJ, 126, 1090
Davis P. J., Kolb U., Willems B., 2010, MNRAS, 403, 179
Drechsel H. et al., 2001, A&A, 379, 893
Eastman J., Siverd R., Gaudi B. S., 2010, PASP, 122, 935
Faillace G., Pulley D., Watkins A., Mallett J., Sharp I., Mai X., 2019, preprint (arXiv:1911.00125)
Fitzpatrick E. L., 1999, PASP, 111, 63
Foreman-Mackey D., Hogg D. W., Lang D., Goodman J., 2013, PASP, 125, 306
Geier S., Heber U., Podsiadlowski P., Edelmann H., Napiwotzki R., Kupfer T., Müller S., 2010, A&A, 519, A25
Goodman J., Weare J., 2010, Commun. Appl. Math. Comput. Sci., 5, 65
Greenstein J. L., 1987, in Philip A. G. D., Hayes D. S., Liebert J. W., eds, IAU Colloq. 95, Second Conference on Faint Blue Stars. Davis Press, Schenectady, NY, p. 3
Han Z., Podsiadlowski P., Maxted P. F. L., Marsh T. R., Ivanova N., 2002, MNRAS, 336, 449
Han Z., Podsiadlowski P., Maxted P. F. L., Marsh T. R., 2003, MNRAS, 341, 669
Han Z., Podsiadlowski P., Lynas-Gray A. E., 2007, MNRAS, 380, 1098
Han Z.-T. et al., 2018, ApJ, 868, 53
Heber U., 2009, ARA&A, 47, 211
Heber U., 2016, PASP, 128, 082001
Hilditch R. W., 2001, An Introduction to Close Binary Stars. Cambridge Univ. Press, Cambridge
Horner J., Hinse T. C., Wittenmyer R. A., Marshall J. P., Tinney C. G., 2012, MNRAS, 427, 2812
Irwin J. B., 1952, ApJ, 116, 211
Kao M. M., Hallinan G., Pineda J. S., Stevenson D., Burgasser A., 2018, ApJS, 237, 25
Kilkenny D., Marang F., Menzies J. W., 1994, MNRAS, 267, 535
Kiss L. L., Csák B., Szatmáry K., Furész G., Sziládi K., 2000, A&A, 364, 199
Kruspe R., Schuh S., Traulsen I., 2007, Inf. Bull. Var. Stars, 5796, #1
Laine M., Tamminen J., 2008, Atmos. Chem. Phys., 8, 7697
Lanza A. F., 2020, MNRAS, 491, 1820
Lasker B. M. et al., 2008, AJ, 136, 735
Law N. M. et al., 2015, PASP, 127, 234
Law N. M., Fors O., Ratzloff J., Corbett H., del Ser D., Wulfken P., 2016, Proc. SPIE, 9906, 99061M
Lee J. W., Kim S.-L., Kim C.-H., Koch R. H., Lee C.-U., Kim H.-I., Park J.-H., 2009, AJ, 137, 3181
Lee J. W., Hinse T. C., Youn J.-H., Han W., 2014, MNRAS, 445, 2331
Liddle A. R., 2007, MNRAS, 377, L74
Lynas-Gray A. E., 2004, Ap&SS, 291, 197
McCarthy D. D., Hackman C., Nelson R. A., 2008, AJ, 136, 1906
Maíz Apellániz J., Weiler M., 2018, A&A, 619, A180
Mayor M., Queloz D., 1995, Nature, 378, 355
Menzies J. W., Marang F., 1986, in Hearnshaw J. B., Cottrell P. L., eds, Proc. IAU Symp. 118, Instrumentation and Research Programmes for Small Telescopes. Reidel, Dordrecht, p. 305
Navarrete F. H., Schleicher D. R. G., Zamponi Fuentealba J., Völschow M., 2018, A&A, 615, A81
Nelemans G., Tout C. A., 2005, MNRAS, 356, 753
Németh P., Kiss L. L., Sarneczky K., 2005, Inf. Bull. Var. Stars, 5599
Niarchos P. G., Gazeas K. D., Manimanis V. N., 2003, in Sterken C., ed., ASP Conf. Ser. Vol. 292, Interplay of Periodic, Cyclic and Stochastic Variability in Selected Areas of the H-R Diagram. Astron. Soc. Pac., San Francisco, p. 129
Odell A. W., Gooding R. H., 1986, Celest. Mech., 38, 307
O'Toole S. J., Jordan S., Friedrich S., Heber U., 2005, A&A, 437, 227
Preece H. P., Tout C. A., Jeffery C. S., 2018, MNRAS, 481, 715
Preece H. P., Tout C. A., Jeffery C. S., 2019, MNRAS, 485, 2889
Pulley D., Faillace G., Smith D., Watkins A., von Harrach S., 2018, A&A, 611, A48
Qian S.-B. et al., 2009, ApJ, 695, L163
Qian S.-B. et al., 2010, Ap&SS, 329, 113
Qian S.-B. et al., 2013, MNRAS, 436, 1408
Ratzloff J. K. et al., 2020, ApJ, 890, 126
Reiners A., 2012, Living Rev. Sol. Phys., 9, 1
Schleicher D. R. G., Dreizler S., 2014, A&A, 563, A61
Schleicher D. R. G., Dreizler S., Völschow M., Banerjee R., Hessman F. V., 2015, Astron. Nachr., 336, 458
Schwarz G., 1978, Ann. Stat., 6, 461
Skrutskie M. F. et al., 2006, AJ, 131, 1163
Song S., Mai X., Mutel R. L., Pulley D., Faillace G., Watkins A., 2019, AJ, 157, 184
Völschow M., Schleicher D. R. G., Perdelwitz V., Banerjee R., 2016, A&A, 587, A34

Völschow M., Schleicher D. R. G., Banerjee R., Schmitt J. H. M. M., 2018, A&A, 620, A42
Wilkinson D. M., Maraston C., Goddard D., Thomas D., Parikh T., 2017, MNRAS, 472, 4297
Wood J. H., Saffer R., 1999, MNRAS, 305, 820
Wood J. H., Zhang E.-H., Robinson E. L., 1993, MNRAS, 261, 103
Xiong H., Chen X., Podsiadlowski P., Li Y., Han Z., 2017, A&A, 599, A54
Zorotovic M., Schreiber M. R., 2013, A&A, 549, A95
Zwicky F., 1965a, in Luyten W. J., ed., First Conference on Faint Blue Stars. Univ. Minnesota, Minneapolis, MN, p. 3
Zwicky F., 1965b, in Luyten W. J., ed., First Conference on Faint Blue Stars. Univ. Minnesota, Minneapolis, MN, p. 114
Zwolak J. W., Boggs P. T., Watson L. T., 2007, ACM Trans. Math. Software, 33, 27

SUPPORTING INFORMATION

Supplementary data are available at *MNRAS* online.

supplementary.data

Please note: Oxford University Press is not responsible for the content or functionality of any supporting materials supplied by the authors. Any queries (other than missing material) should be directed to the corresponding author for the article.

APPENDIX A: V470 CAM ECLIPSE TIMES

All good quality primary, and some secondary, eclipse times for V470 Cam at the time of writing are listed in Table A1. Columns 1, 5, and 9 give eclipse numbers determined using Equation (2). Columns 2, 6, and 10 give observed barycentric dynamical times (BJD_{TDB}; Eastman et al. 2010) obtained from the literature, or determined as described above in the case of observations reported in this paper. Secondary eclipses were distinguished by a '.5' appended to the eclipse number. Columns 3, 7, and 11 list observed minus calculated (O − C) BJD_{TDB} residuals for elliptical orbits in units of 10^{-5} d. Literature citations were indicated by a numerical code in columns 4, 8, and 12: 1 – Drechsel et al. (2001); 2 – Niarchos, Gazeas & Manimanis (2003); 3 – Qian et al. (2009); 4 – Qian et al. (2010); 5 – Çamurdan et al. (2012); 6 – Beuermann et al. (2012); 7 – Qian et al. (2013); 8 – Pulley et al. (2018); 9 – Bogensberger et al. (2017, 2018); 10 – Németh et al. (2005); 11 – Kruspe, Schuh & Traulsen (2007); 12 – this paper; and 13 – Faillace et al. (2019). We noted that (O − C) residuals Çamurdan et al. list in their table 3 could only be recovered with the ephemeris Drechsel et al. print, which is not appropriate when BJD_{TDB} is used. As already mentioned, three eclipse times which other authors publish but do not use were omitted from Table A1.

Table A1. Eclipse times.

N	BJD_{TDB} – 245 0000	O − C	Ref.	*N*	BJD_{TDB} – 245 0000	O − C	Ref.	*N*	BJD_{TDB} – 245 0000	O − C	Ref.
−2509	1582.78327(064)	− 86.3	6	31288	4815.35233(014)	− 133.4	3	40272.5	5674.69059(004)	− 46.9	6
0	1822.76051(005)	− 101.7	1	31308	4817.26516(039)	− 143.7	3	40273	5674.73836(003)	− 52.8	6
10	1823.71716(010)	− 83.3	1	31309	4817.36106(039)	− 118.4	3	40355.5	5682.62908(012)	− 65.9	6
291	1850.59374(011)	− 95.6	1	31435	4829.41176(019)	− 197.1	3	40356	5682.67709(003)	− 46.9	6
292	1850.68939(012)	− 95.5	1	31527	4838.21172(012)	− 150.3	3	40429	5689.65926(003)	− 50.7	6
585	1878.71389(003)	− 91.5	1	31602	4845.38518(027)	− 153.8	7	40475	5694.05902(003)	− 49.2	7
1009	1919.26773(020)	− 124.7	1	31602	4845.38531(018)	− 140.8	7	40960	5740.44775(002)	− 39.3	7
1010	1919.36343(100)	− 119.3	1	32124	4895.31259(032)	− 168.1	7	41430	5785.40178(002)	− 29.4	7
1011	1919.45933(010)	− 94.0	1	32124	4895.31268(029)	− 159.1	7	41488	5790.94929(003)	− 29.1	6
1398	1956.47453(130)	− 98.6	1	32131	4895.98235(006)	− 145.3	4	41519	5793.91436(003)	− 27.0	6
1399	1956.57043(110)	− 73.3	1	32131.5	4896.02998(044)	− 164.6	4	41529.5	5794.91860(004)	− 31.9	6
1815	1996.35933(010)	− 83.2	1	32303	4912.43363(016)	− 139.3	7	41540	5795.92290(003)	− 30.6	6
1825	1997.31573(010)	− 89.8	1	32448	4926.30256(015)	− 123.2	4	41624	5803.95726(003)	− 26.4	6
5191	2319.26257(065)	− 62.2	2	32449	4926.39793(013)	− 149.9	4	41683	5809.60044(004)	− 23.6	6
5191.5	2319.31052(082)	− 49.6	2	32605	4941.31919(031)	− 112.7	4	41903	5830.64273(003)	− 21.4	6
5192	2319.35793(061)	− 90.9	2	32660	4946.57946(013)	− 141.4	4	41962	5836.28592(002)	− 17.8	7
5192.5	2319.40614(088)	− 52.2	2	32696	4950.02263(011)	− 152.4	4	42250	5863.83220(002)	− 13.7	6
5201.5	2320.26677(091)	− 71.2	2	32769.5	4957.05245(010)	− 173.3	4	42251	5863.92783(002)	− 15.3	6
5205	2320.60163(070)	− 61.5	2	33484	5025.39256(040)	− 115.9	4	42371	5875.40539(009)	− 19.3	7
12426.5	3011.31546(040)	102.3	10	33757	5051.50394(024)	− 131.7	4	42400	5878.17925(004)	− 8.7	7
12427	3011.36386(010)	159.9	10	33778	5053.51270(016)	− 113.6	4	42401	5878.27484(004)	− 14.3	7
12427.5	3011.41126(040)	117.6	10	33881	5063.36389(003)	− 155.2	4	42461	5884.01368(003)	− 10.4	6
13053.5	3071.28656(030)	168.0	10	33946	5069.58102(006)	− 145.5	6	42596	5896.92599(002)	− 9.4	6
13054	3071.33416(010)	145.7	10	33977	5072.54605(006)	− 147.3	6	42682	5905.15165(008)	− 4.5	7
13054.5	3071.38236(040)	183.4	10	34164	5090.43194(002)	− 150.6	4	42787	5915.19458(005)	− 1.5	7
13055	3071.42986(010)	151.0	10	34288	5102.29216(002)	− 147.2	4	42818	5918.15961(005)	− 3.2	7
23616.5	4081.60071(018)	32.6	3	34541	5126.49077(002)	− 146.8	7	42885	5924.56795(001)	− 1.8	7
23617	4081.64764(018)	− 56.7	3	34664	5138.25524(004)	− 153.7	7	42924	5928.29825(011)	6.2	7
24085	4126.41047(110)	− 36.8	11	34798.5	5151.11975(009)	− 150.2	7	42976	5933.27186(005)	4.6	7
24085.5	4126.45877(110)	10.9	11	34812	5152.41103(001)	− 145.2	7	43026	5938.05435(017)	20.2	7
24086	4126.50567(110)	− 81.5	11	34940	5164.65382(002)	− 143.4	7	43238	5958.33123(001)	− 1.0	7
24086.5	4126.55407(110)	− 23.8	11	35375	5206.26018(003)	− 137.0	7	43321	5966.26989(004)	− 2.3	7
24087	4126.60147(240)	− 66.1	11	35534	5221.46801(002)	− 135.9	7	43748	6007.11103(010)	− 0.9	7
27157	4420.23612(015)	− 122.2	3	35640	5231.60654(001)	− 137.4	7	43998	6031.02263(010)	− 7.4	7
27157.5	4420.28437(025)	− 79.6	3	35932	5259.53538(002)	− 135.8	7	44264	6056.46490(002)	18.3	7
27908	4492.06689(018)	− 109.6	3	35982	5264.31775(001)	− 132.1	7	44427	6072.05530(010)	17.7	7
27908.5	4492.11474(022)	− 106.0	3	36021	5268.04800(004)	− 129.1	7	44808	6108.49668(002)	17.8	7
27909	4492.16254(018)	− 109.3	3	36233	5288.32509(002)	− 129.2	7	44944	6121.50466(001)	21.1	7
28173	4517.41288(034)	− 145.9	3	36282	5293.01179(007)	− 127.9	7	45571	6181.47516(002)	25.2	7
28174	4517.50899(037)	− 100.6	3	36282	5293.01191(009)	− 115.9	7	45894	6212.36907(002)	28.9	7
29480	4642.42317(027)	− 135.4	3	36282.5	5293.05951(009)	− 138.2	7	45936	6216.38604(009)	9.9	7
29658	4659.44872(047)	− 90.8	3	36282.5	5293.05972(014)	− 117.2	7	45966	6219.25553(008)	19.0	7
29919	4684.41146(024)	− 194.4	3	36914	5353.46050(004)	− 125.7	7	46008	6223.27260(008)	10.0	7
29920	4684.50727(024)	− 178.1	3	38168	5473.40172(001)	− 94.7	7	46124	6234.36786(007)	34.6	7
30244	4715.49760(020)	− 95.7	3	38232	5479.52310(001)	− 95.3	7	46176	6239.34164(014)	50.0	7
30245	4715.59242(023)	− 178.3	3	38544	5509.36491(006)	− 90.1	7	46186	6240.29798(007)	37.3	7
30276	4718.55688(041)	− 237.0	3	38816	5535.38087(002)	− 83.2	7	46196	6241.25432(009)	24.6	7
30388.5	4729.31819(015)	− 131.8	3	38847	5538.34585(001)	− 89.9	5	46311	6252.25371(008)	27.0	7
30389	4729.36575(015)	− 158.1	3	38848	5538.44149(002)	− 90.6	5	46342	6255.21875(009)	26.3	7
30514	4741.32165(008)	− 150.3	3	38849	5538.53715(002)	− 89.2	5	46552	6275.30470(010)	41.3	7
30514.5	4741.36934(011)	− 164.6	3	38850	5538.63280(002)	− 88.9	5	46750	6294.24263(003)	30.4	7
30556	4745.33878(020)	− 153.2	3	38858	5539.39798(002)	− 88.2	5	46781	6297.20765(010)	27.7	7
30716	4760.64311(032)	− 67.7	3	38860	5539.58928(002)	− 87.5	5	47125	6330.11019(008)	36.4	7
30724	4761.40726(023)	− 170.0	3	39074	5560.05782(006)	− 72.1	7	47459	6362.05607(006)	25.7	7
30921	4780.24979(009)	− 155.2	3	39098.5	5562.40118(008)	− 70.4	7	47491	6365.11698(008)	47.4	7
30921	4780.25022(015)	− 112.2	3	39153	5567.61384(002)	− 78.7	7	47511.5	6367.07761(019)	34.7	7
30922	4780.34498(034)	− 200.9	3	39716	5621.46305(001)	− 64.7	7	47574	6373.05561(020)	43.1	7
31214	4808.27411(034)	− 170.2	3	39983	5647.00063(010)	− 72.5	7	47648	6380.13340(009)	36.7	7
31215	4808.36996(031)	− 149.8	3	40057	5654.07861(004)	− 59.8	7	47871	6401.46260(002)	36.1	7
31237	4810.47457(020)	− 111.5	3	40230	5670.62555(003)	− 52.9	6	47902	6404.42757(002)	28.4	7
31238	4810.57074(030)	− 59.1	3	40251	5672.63418(003)	− 47.9	6	47953	6409.30558(001)	31.4	7
31287	4815.25657(010)	− 144.7	3	40272	5674.64270(003)	− 53.8	6	48194	6432.35631(002)	19.7	7

Table A1 – *continued*

N	BJD_{TDB} – 245 0000	O − C	Ref.	*N*	BJD_{TDB} – 245 0000	O − C	Ref.	*N*	BJD_{TDB} – 245 0000	O − C	Ref.
49329	6540.91541(007)	32.9	8	58889	7455.29693(003)	− 33.1	8	62267	7778.39179(019)	5.5	9
49601	6566.93122(008)	24.6	8	58953	7461.41837(011)	− 27.8	8	62289	7780.49588(010)	− 8.2	9
49684	6574.87002(008)	37.2	8	58994	7465.34007(016)	− 9.2	8	62475	7798.28598(025)	− 26.4	8
50009	6605.95528(002)	46.5	8	59204	7485.42574(008)	− 22.4	8	62476	7798.38191(021)	2.0	8
50228	6626.90166(011)	22.5	8	59214	7486.38213(017)	− 30.1	8	62477	7798.47746(012)	− 7.7	8
50256	6629.57962(005)	7.8	8	59235	7488.39075(006)	− 26.1	8	62528	7803.35541(013)	− 10.8	8
50275	6631.39723(005)	40.1	8	59445	7508.47673(018)	− 8.3	8	62530	7803.54665(004)	− 16.1	8
50275.5	6631.44496(012)	30.8	8	60830	7640.94726(006)	− 19.9	8	62790	7828.41475(007)	− 19.7	8
50276	6631.49269(017)	21.5	8	61133	7669.92822(005)	− 18.3	8	62843	7833.48411(003)	− 11.1	8
50525.5	6655.35596(018)	− 35.9	8	61672	7721.48180(003)	− 16.2	8	62844	7833.57974(006)	− 12.8	8
50526	6655.40458(007)	43.7	8	61672	7721.48187(010)	− 9.2	9	62884	7837.40559(002)	− 14.5	8
50526.5	6655.45255(017)	58.4	8	61673	7721.57747(010)	− 13.8	9	62884	7837.40560(009)	− 13.5	8
50527	6655.50000(006)	21.1	8	61674	7721.67300(010)	− 25.5	9	62885	7837.50123(004)	− 15.2	8
50603.5	6662.81735(014)	59.1	8	61682	7722.43823(007)	− 19.8	8	62886	7837.59686(006)	− 16.8	8
51153	6715.37491(006)	30.6	8	61682	7722.43823(010)	− 19.8	9	62894	7838.36206(003)	− 14.2	8
51184	6718.33981(005)	15.9	8	61684	7722.62960(010)	− 12.2	9	62895	7838.45773(006)	− 11.9	8
51241	6723.79173(002)	21.9	8	61685	7722.72519(010)	− 17.8	9	62915	7840.37059(009)	− 19.2	8
51408	6739.76486(002)	35.5	8	61692	7723.39478(010)	− 11.5	9	62957	7844.38771(007)	− 23.3	8
51414	6740.33939(006)	100.5	8	61693	7723.49048(010)	− 6.2	9	62978	7846.39644(004)	− 8.3	8
51415	6740.43437(011)	33.8	8	61694	7723.58603(010)	− 15.8	9	63072	7855.38738(016)	6.9	8
51418	6740.72115(009)	17.8	8	61725	7726.55109(010)	− 14.5	9	63145	7862.36961(008)	9.2	8
51784.5	6775.77545(013)	− 2.6	8	61726	7726.64669(010)	− 19.2	9	63187	7866.38662(004)	− 5.9	8
51805	6777.73635(004)	11.7	8	61734	7727.41193(010)	− 12.6	9	63188	7866.48217(004)	− 15.5	8
51826	6779.74500(004)	18.7	8	61922	7745.39362(010)	− 1.1	9	63198	7867.43868(005)	− 11.2	8
53605	6949.90040(003)	16.0	8	61925	7745.68042(010)	− 15.1	9	63365	7883.41174(004)	− 4.7	8
53710	6959.94328(004)	14.0	8	61934	7746.54140(010)	0.9	9	63366	7883.50738(005)	− 5.4	8
53710.5	6959.99096(011)	− 0.4	8	61963	7749.31504(010)	− 10.5	9	63376	7884.46375(005)	− 15.1	8
54023	6989.88095(017)	40.2	8	61964	7749.41063(010)	− 16.1	9	63377	7884.55972(006)	17.2	8
54250	7011.59222(021)	− 12.3	8	61966	7749.60214(010)	5.5	9	63378	7884.65498(002)	− 21.4	8
54271	7013.60107(005)	14.7	8	61967	7749.69761(010)	− 12.1	9	63491	7895.46315(004)	− 11.9	8
54342	7020.39191(007)	7.3	8	61974	7750.36731(015)	5.2	8	65116	8050.88911(004)	− 1.8	13
54479	7033.49544(007)	0.9	8	61984	7751.32369(010)	− 3.5	9	65174	8056.43662(006)	− 0.6	13
54480	7033.59108(006)	0.3	8	61985	7751.41928(010)	− 9.2	9	65320	8070.40091(024)	− 13.8	13
54480.5	7033.63876(021)	− 14.1	8	61988	7751.70625(010)	− 6.2	9	65500	8087.61759(009)	14.2	12
54481	7033.68675(012)	2.6	8	62036	7756.29714(010)	− 21.2	9	65582	8095.46035(009)	− 12.6	12
54530	7038.37346(003)	4.9	8	62037	7756.39272(010)	− 27.9	8	65592	8096.41710(009)	15.7	12
54532	7038.56464(004)	− 6.4	8	62037	7756.39274(004)	− 25.9	9	65594	8096.60819(009)	− 4.6	12
54533	7038.66039(003)	3.9	8	62038	7756.48846(005)	− 18.6	8	65595	8096.70399(009)	10.7	12
54543	7039.61689(008)	7.2	8	62038	7756.48853(010)	− 11.6	9	65626	8099.66882(009)	− 11.0	12
55192	7101.69132(002)	− 18.8	8	62039	7756.58409(004)	− 20.2	8	65791	8115.45069(009)	5.8	12
55255.5	7107.76482(014)	− 25.2	8	62040	7756.67977(008)	− 16.9	8	65792	8115.54630(009)	2.1	12
55418.5	7123.35571(016)	23.1	8	62059	7758.49707(010)	− 15.6	9	65801	8116.40710(009)	0.1	12
55419	7123.40318(005)	− 12.3	8	62060	7758.59270(010)	− 17.2	9	65802	8116.50273(009)	− 1.6	12
55460.5	7127.37244(020)	− 20.0	8	62061	7758.68844(010)	− 7.9	9	65843	8120.42430(009)	4.0	12
55461	7127.42034(006)	− 12.3	8	62069	7759.45337(010)	− 32.3	9	65844	8120.51991(009)	0.4	12
55502	7131.34191(007)	− 6.6	8	62070	7759.54925(010)	− 8.9	9	65845	8120.61565(009)	9.7	12
55502.5	7131.38979(016)	− 1.0	8	62214	7773.32240(016)	− 6.1	8	65886	8124.53695(009)	− 11.7	12
55503	7131.43748(003)	− 14.3	8	62215	7773.41796(020)	− 14.7	8	65887	8124.63262(009)	− 9.4	12
55524	7133.44612(004)	− 8.3	8	62224	7774.27881(011)	− 11.8	8	66000	8135.44080(009)	1.2	12
55534	7134.40251(002)	− 16.0	8	62225	7774.37449(005)	− 8.4	8	66002	8135.63194(009)	− 14.2	12
55534.5	7134.45017(009)	− 32.3	8	62226	7774.47002(011)	− 20.1	8	66030	8138.31001(009)	− 17.9	12
57443	7316.99185(004)	− 32.0	8	62235	7775.33099(010)	− 5.1	9	66093	8144.33606(003)	12.6	13
57949	7365.38916(001)	− 22.7	8	62236	7775.42653(010)	− 15.8	9	66094	8144.43145(010)	− 12.4	13
57950	7365.48480(003)	− 23.4	8	62237	7775.52231(010)	− 2.4	9	66095	8144.52736(004)	13.6	13
57950.5	7365.53269(009)	− 16.7	8	62245	7776.28748(010)	− 2.8	9	66096	8144.62296(003)	9.0	13
58262.5	7395.37443(013)	− 18.9	8	62246	7776.38302(010)	− 13.4	9	66157	8150.45742(009)	10.3	12
58263	7395.42219(007)	− 25.3	8	62247	7776.47853(010)	− 27.1	9	66168	8151.50955(009)	11.9	12
58347	7403.45664(006)	− 12.3	8	62266	7778.29590(025)	− 18.8	8	66273	8161.55241(003)	8.0	13
58387.5	7407.33031(028)	− 14.4	8	62266	7778.29603(010)	− 5.8	9	66282	8162.41323(005)	7.7	13
58388	7407.37821(010)	− 6.7	8	62266.5	7778.34372(018)	− 19.1	8	66283	8162.50902(008)	21.9	13
58544	7422.29875(010)	− 40.8	8	62267	7778.39153(006)	− 20.5	8	66805	8212.43657(013)	20.7	13
58619	7429.47249(006)	− 16.9	8	62267	7778.39163(010)	− 10.5	8	66930	8224.39231(016)	10.9	13

Table A1 – *continued*

N	BJD_{TDB} – 245 0000	O − C	Ref.	*N*	BJD_{TDB} – 245 0000	O − C	Ref.	*N*	BJD_{TDB} – 245 0000	O − C	Ref.
66952	8226.49659(028)	15.8	13	69942	8512.48037(024)	35.6	13	70788	8593.39747(010)	36.6	13
67223	8252.41703(025)	35.3	13	69962	8514.39325(010)	30.4	13	70893	8603.44046(008)	45.8	13
67286	8258.44257(020)	14.9	13	69963	8514.48899(011)	39.7	13	71217	8634.42995(018)	42.2	13
68959	8418.45965(013)	32.8	13	70442	8560.30375(005)	39.7	13	71991	8708.46055(017)	48.6	13
69032	8425.44180(016)	26.8	13	70444	8560.49499(003)	34.8	13	72201	8728.54636(004)	48.6	13
69188	8440.36281(018)	40.1	13	70516	8567.38180(010)	59.5	13	72201	8728.54633(004)	46.1	13
69189	8440.45827(021)	21.4	13	70517	8567.47739(019)	53.6	13	72264	8734.57212(005)	50.4	13
69418	8462.36147(012)	31.9	13	70528	8568.52934(003)	37.1	13	72326	8740.50220(010)	49.5	13
69659	8485.41226(008)	26.5	13	70537	8569.39025(007)	46.5	13				
69733	8492.49016(006)	31.0	13	70726	8587.46737(013)	36.1	13				

APPENDIX B: PARAMETER CORRELATIONS

Parameter correlations are shown in corner plots, Figs B1–B3. In order to provide legible axis labelling, and for the purpose of including in corner plots only, we have scaled each parameter to lie in the range $-1.0 \leq P \leq +1.0$. Scalings producing the desired result are presented in Table B1 and from which parameter values may be recovered using

$$P = \Delta P \, P_{\rm scaled} + P_0. \tag{B1}$$

As an example, for the value of a_0 plotted as 0.2, evaluate $0.2 \times 1.521499999626 \times 10^{-04} + 1.822761512150 \times 10^{+03}$ to obtain 1822.79194.

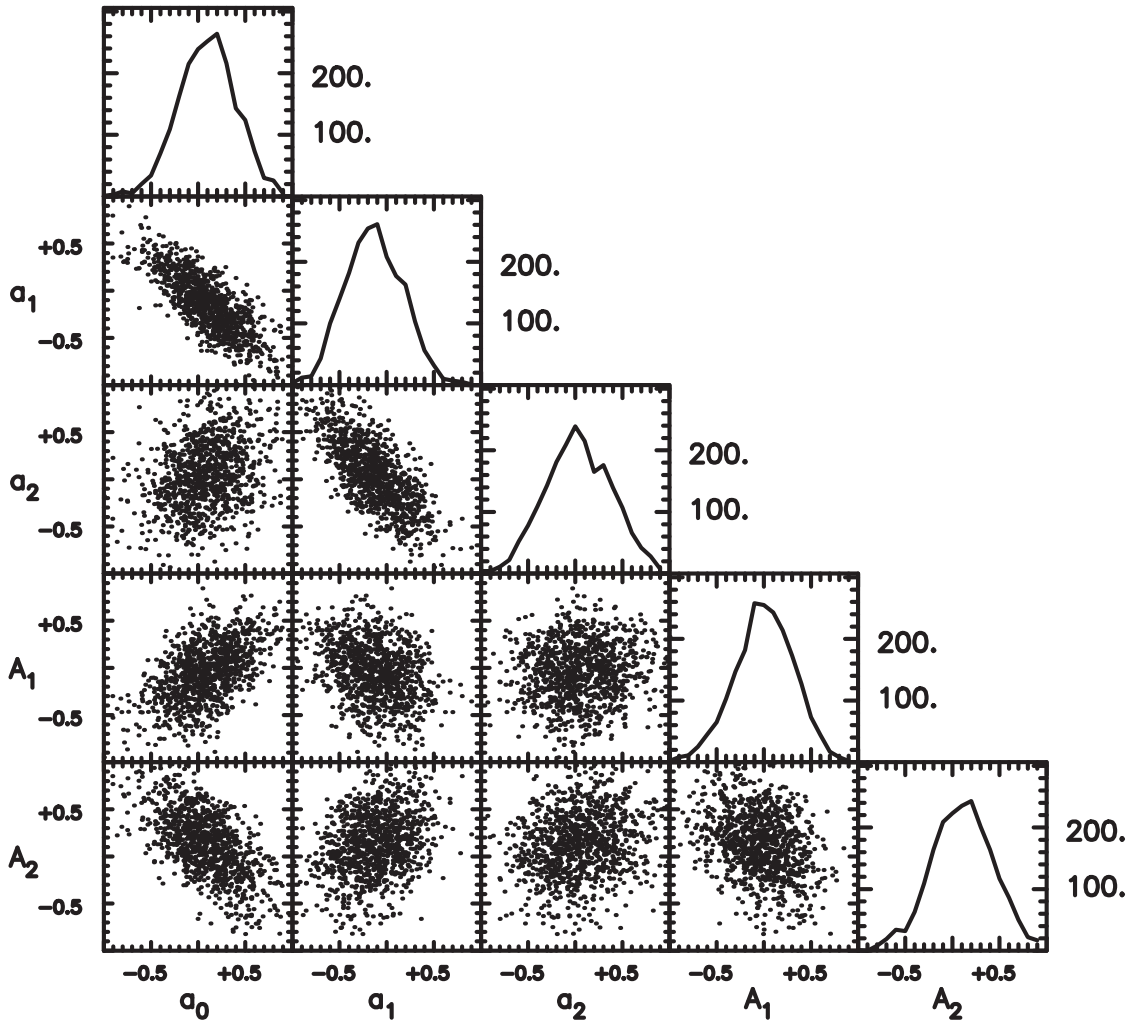

Figure B1. Correlations between, and distributions of, scaled sample ephemeris coefficient values and V470 Cam binary reflex motion amplitudes produced by OB1 and OB2 assuming elliptical orbits.

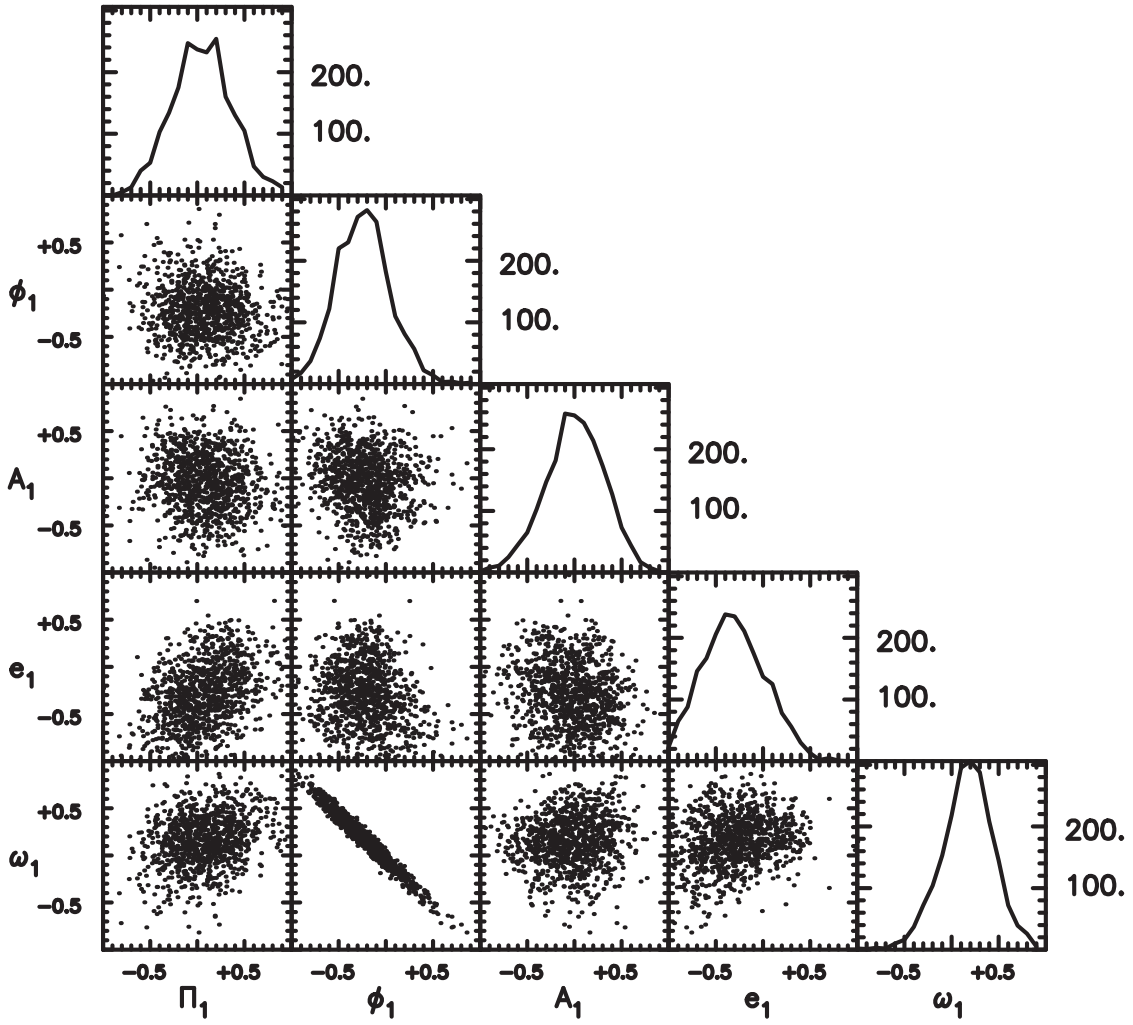

Figure B2. Correlations between, and distributions of, scaled sample elliptical orbital parameters for the V470 Cam binary reflex motion induced by OB1.

Table B1. Elliptical orbits corner plot parameter scaling.

Parameter	ΔP	P_0
a_0	$1.521499999626 \times 10^{-04}$	$+1.822761512150 \times 10^{+03}$
a_1	$4.213500000294 \times 10^{-09}$	$+9.564663074450 \times 10^{-02}$
a_2	$3.587838052500 \times 10^{-14}$	$+3.815702713250 \times 10^{-13}$
Π_1	$9.324899375000 \times 10^{+02}$	$+2.995763229550 \times 10^{+04}$
ϕ_1	$1.370157844995 \times 10^{+00}$	$-1.750624207805 \times 10^{+00}$
A_1	$5.990117655500 \times 10^{-05}$	$+8.540972743950 \times 10^{-04}$
Π_2	$1.946303974000 \times 10^{+03}$	$+5.048827560900 \times 10^{+04}$
ϕ_2	$4.085914021500 \times 10^{-01}$	$-1.677636188150 \times 10^{+00}$
A_2	$6.061772427000 \times 10^{-05}$	$-7.606908568100 \times 10^{-04}$
e_1	$1.109566444537 \times 10^{-01}$	$+1.111001418263 \times 10^{-01}$
ω_1	$1.494121175750 \times 10^{+00}$	$-8.986555485000 \times 10^{-02}$
e_2	$1.484532678650 \times 10^{-01}$	$+4.729353983950 \times 10^{-01}$
ω_2	$3.774965695400 \times 10^{-01}$	$-1.374945333160 \times 10^{+00}$

For the purpose of plotting sample parameter value distributions in corner plot (Figs B1–B3) uppermost panels, we collected scaled values for each parameter sample value into twenty bins centred on -0.95, -0.85, ..., -0.05, $+0.05$, ..., $+0.95$. Corresponding abscissae were plotted at the bottom of each panel column. Numbers of sample values in each bin were entered on the right-hand ordinate axes.

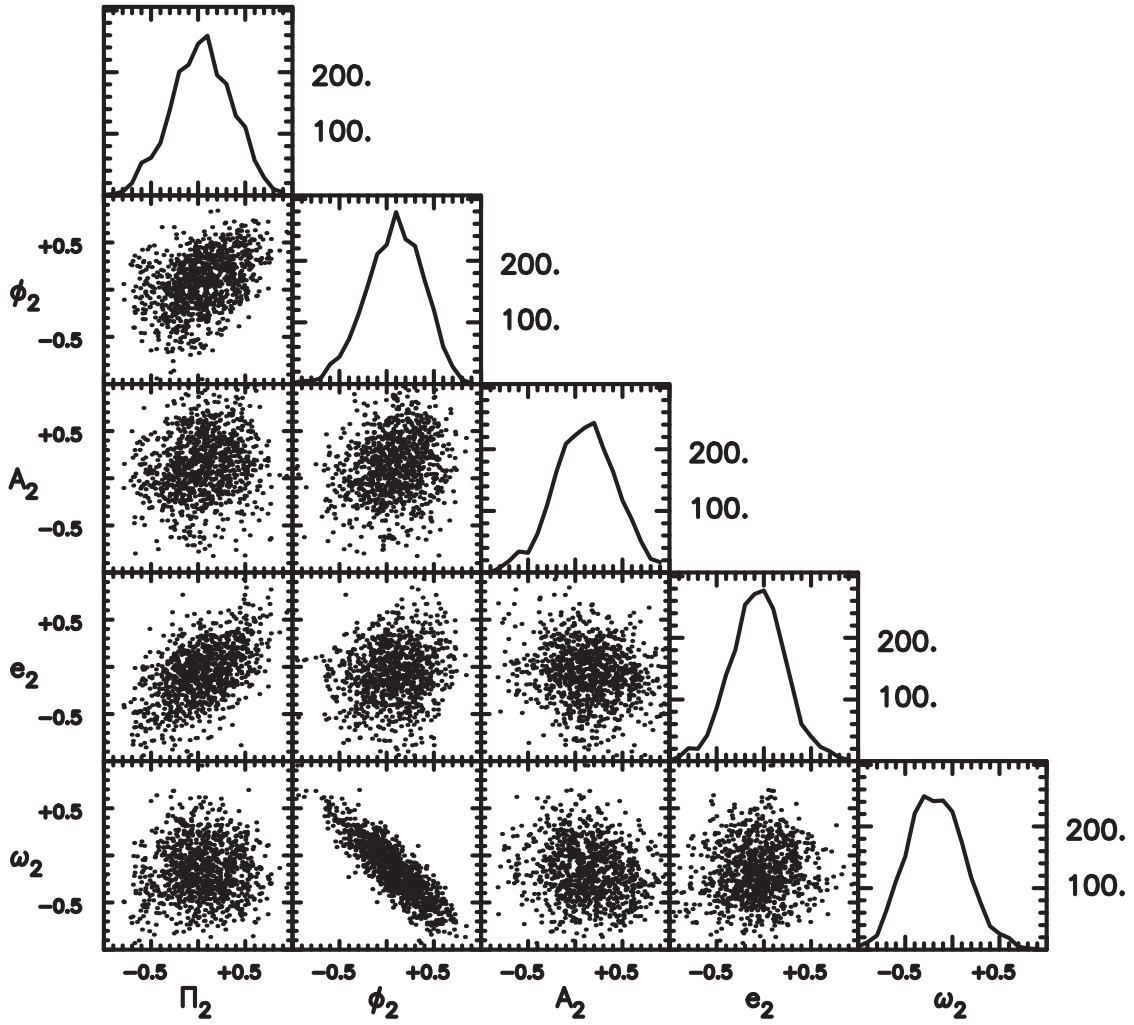

Figure B3. Correlations between, and distributions of, scaled sample elliptical orbital parameters for the V470 Cam binary reflex motion induced by OB2.

APPENDIX C: BAYESIAN INFERENCE CRITERION

As was assumed with MCMC sampling, the time at which each eclipse number N was observed (t_N) is sampled from a Gaussian distribution and each is independent. The likelihood ($L_{\rm c,\,e}$) that Table A1 eclipse times were obtained is then

$$\ln L_{\rm c,e} = -\frac{1}{2}\sum_{N}^{N_{\rm tot}}\left[\frac{t_N - T_{\rm c,e}(N)}{\sigma_N}\right]^2 - \sum_{N}^{N_{\rm tot}}\left[\sigma_N\sqrt{2\pi}\right], \qquad \text{(C1)}$$

where the subscripts c and e, respectively, denote the circular and elliptical orbit cases. $N_{\rm tot}$ is the total number of eclipse times and σ_N the standard deviation in t_N. Parameters given for OB1 and OB2 by MCMC sampling substituted into Equations (6) and (7) gave $\tau_{\rm c}(N)$ and $\tau_{\rm e}(N)$, respectively, for both objects, which in turn gave predicted $T_{\rm c,\,e}(N)$ values using Equation (9).

Schwarz (1978) introduces BIC evaluations using expressions which, in our notation, are of the form

$$\mathrm{BIC}_{\rm c,e} = -2\ln L_{\rm c,e} + k_{\rm c,e}\ln N_{\rm tot}, \qquad \text{(C2)}$$

where again the subscripts c and e, respectively, identify circular and elliptical orbit cases, with $k_{\rm c,\,e}$ denoting numbers of parameters upon which the corresponding fit was dependent. Equation (C1) may be rewritten as

$$-2\ln L_{\rm c,e} = \chi^2 + 2K, \qquad \text{(C3)}$$

where

$$K = \sum_{N}^{N_{\rm tot}}\left[\sigma_N\sqrt{2\pi}\right]. \qquad \text{(C4)}$$

As defined by Equation (C4), K is model-independent and so on combining Equations (C2) and (C3), we have followed Wilkinson et al. (2017, their equation 1) and adopted the statistic

$$\mathrm{BIC}_{\rm c,e} - 2K = \chi^2 + k_{\rm c,e}\ln N_{\rm tot}. \qquad \text{(C5)}$$

The right-hand side of Equation (C5) is always positive and represents the familiar χ^2 statistic augmented by a 'penalty' for using additional fit parameters in a model. Therefore, in comparing models, a smaller value of $\mathrm{BIC}_{\rm c,\,e} - 2K$ was preferred.

This paper has been typeset from a TEX/LATEX file prepared by the author.